Journal of Sustainable Construction Materials and Technologies

Volume 10 | Issue 4 Article 10

2025

Curing Duration Optimization to Reduce Shrinkage Cracking in One-Part Alkali-Activated Slag Concrete

A. Sadrmomtazi
Professor, Department of Civil Engineering, Faculty of Engineering, University of Guilan, Rasht, Iran

H. Zanganeh
Ph.D. Candidate, Department of Civil Engineering, Faculty of Engineering, University of Guilan, Rasht, Iran, Hamedzanganeh@gmail.com

JOURNAL OF SUSTAINABLE CONSTRUCTION MATERIALS AND TECHNOLOGIES 2025;10:584–601

RESEARCH ARTICLE

Curing Duration Optimization to Reduce Shrinkage Cracking in One-Part Alkali-Activated Slag Concrete

A. Sadrmomtazi [a], **H. Zanganeh** [b,*]

[a] Professor, Department of Civil Engineering, Faculty of Engineering, University of Guilan, Rasht, Iran
[b] Ph.D. Candidate, Department of Civil Engineering, Faculty of Engineering, University of Guilan, Rasht, Iran

ABSTRACT

The consequences of inadequate curing on one-part alkali-activated slag concrete (O-AAS) performance relative to ordinary Portland cement concrete (OPCC) have been investigated in this research. Prior to exposure to unsaturated conditions, samples underwent initial moist curing for durations ranging from 24 hours to one year. The testing program included compressive strength evaluation, chloride ion transport analysis, and measurement of free and restrained shrinkage. In addition, cylindrical cores were extracted from concrete columns to assess internal strength and chloride penetration resistance. Under unsaturated exposure, O-AAS exhibited a strength-aging phenomenon, with up to a 37% decrease in compressive strength over 360 days, whereas OPCC maintained stable strength. Reduced curing durations at ambient temperature resulted in lower compressive strength and increased chloride migration coefficients. With adequate curing, long-term performance was comparable to that under continuous saturated conditions. Extending initial curing from 24 hours to one week decreased 28-day free shrinkage by 18.1% and restrained crack width by 56.0%. Core analysis revealed that inadequate curing led to microcrack development in O-AAS, while sufficient curing duration resulted in performance matching that of continuously saturated specimens. For OPCC, core performance did not differ significantly in varying curing regimes. Early-age curing is critical for mitigating shrinkage damage and preserving long-term durability in O-AAS concretes, especially under unsaturated environmental conditions.

Keywords: One-Part Alkali-Activated Slag Concrete, Rapid Chloride migration Test, Curing Duration, Shrinkage microcrack, Long-term performance

1. Introduction

The construction industry's imperative to reduce carbon emissions has positioned alkali-activated materials (AAMs) as promising sustainable alternatives to conventional Portland cement systems, as cement production accounts for approximately 8% of global carbon emissions while AAMs can potentially reduce this figure by up to 80% [1–3]. Among AAM formulations, one-part systems characterized by their "just-add-water" activation mechanism offer significant practical advantages for field applications, eliminating the need to handle liquid activators that pose health hazards to workers [4–8].

Within the category of one-part systems, one-part alkali-activated slag concrete (O-AAS) demonstrates appropriate strength development and competitive mechanical performance with ordinary Portland cement concrete (OPCC) [3, 4, 7], along with lower permeability when cured at ambient temperature [7, 9], making it a suitable choice for cast-in-place applications [3, 4]. The primary challenge in implementing one-part alkali-activated systems based on slag is the fundamental mismatch between strength

Received 30 August 2025; revised 6 December 2025; accepted 20 December 2025.
Available online 30 December 2025

* Corresponding author.
E-mail address: Hamedzanganeh@gmail.com (H. Zanganeh).

https://doi.org/10.29187/2458-973X.1207

development and shrinkage behaviour [4]. While these systems can achieve acceptable compressive strengths at ambient temperature, their high shrinkage can lead to extensive microcracking, which creates pathways for destructive environmental factors, seriously threatening the long-term durability of concrete [3, 4, 10, 11]. This issue is particularly significant in cast-in-place concrete applications where curing duration presents implementation challenges. This challenge stems from fundamental differences in hydration mechanisms between alkali-activated systems and Portland cement.

In structural elements such as pavements, bridge decks, and concrete surfaces directly exposed to air, drying conditions typically dominate as ambient relative humidity is below saturation. According to established standard [12], relative humidity of 50% is considered the standard condition for simulating typical shrinkage behaviour in structural concrete [10, 13]. Under these conditions, moisture evaporation causes drying shrinkage and volumetric changes that can lead to microcrack formation and gradual durability reduction. Although OPCC and alkali-activated concrete (AAS) are affected by drying shrinkage under standard conditions, their responses differ significantly due to variations in hydration chemistry. OPCC primarily produces C-S-H gel, while AAS systems generate C-A-S-H gel with a denser pore network and higher capillary tension. Consequently, AAS mixtures may exhibit drying shrinkage up to six times greater than OPCC, making them more susceptible to microcracking and subsequent performance reduction [10].

In OPCC, microcracks resulting from shrinkage are primarily concentrated in the surface region, with their penetration depth in OPCC concrete limited to a few millimetres [14]; therefore, their effect is only observed on the permeability results of the exposed surface [13] and has no impact on the compressive strength of OPCC specimens [14, 15]. In contrast, AAS concretes, due to higher shrinkage, may have greater microcrack penetration depth, with their effects visible not only on increased permeability [16] but also on long-term compressive strength [17, 18]. Thus, this significant tendency of AAS toward shrinkage-related cracking can create serious challenges for concrete durability and strength.

Numerous studies have reported that AAS experiences significant reductions in compressive strength under unsaturated exposure conditions [17–19]. This strength reduction can vary widely, ranging from approximately 7% to 70%. These studies have utilized different curing durations, indicating that the degree of strength reduction is influenced by varying curing regimes. In this research, the activator-to-slag ratio was determined in such a way that, while maintaining constant water-to-binder ratio, comparable compressive strength was achieved under initial curing conditions in alkaline solution. This methodological approach enables the isolation of curing duration effects from compressive strength variables. Given the lack of systematic studies on the relationship between curing duration and shrinkage behaviour in one-part alkali-activated systems, this research investigates this relationship in O-AAS concrete.

In this study, compressive strength tests, free and restrained shrinkage measurements, and rapid chloride migration tests (RCMT) were conducted, with all tests monitored for up to 360 days. This research aims to enhance the mechanical properties and long-term durability of O-AAS by reducing the effects of shrinkage microcracking. These findings contribute to improving the durability of O-AAS concrete structures and can be considered a step toward achieving sustainable development goals in the construction industry.

2. Materials and methods

2.1. Materials

This research utilized a combination of locally sourced and imported materials, and all components were characterized in accordance with applicable ASTM standards. The binder system was composed of three main components:

- OPC (ordinary Portland cement): Type II Portland cement, sourced from Nahavand Cement Company, met the requirements of ASTM C150 [20].
- GGBFS (Ground Granulated Blast Furnace Slag): Slag was provided by Isfahan Iron Smelting Industries, in accordance with ASTM C989 [21].
- Na_2SiO_3: This anhydrous powder, which served as the solid alkaline activator, was imported from Qingdao Darun Chemical Industries.

Further details regarding the chemical makeup of the binders are provided in Table 1, with their physical attributes outlined in Table 2.

Aggregates were sourced from quarries situated in the south-western region of Tehran. The concrete blend incorporated coarse particles limited to a maximum dimension of 12.5 mm alongside naturally sourced sand serving as the fine component. Both of these aggregates conformed to ASTM C33 [22].

2.2. Mix design and testing procedures

The total binder content was maintained at 450 kg/m^3, and the water-to-binder ratio was set at 0.52

Table 1. Compositional characteristics of binders.

Binders	SiO_2	Al_2O_3	Fe_2O_3	CaO	MgO	SO_3	Na_2O	K_2O	L.O.I.
OPC	20.80	4.80	4.00	63.70	2.10	2.40	0.37	0.85	0.96
GGBFS	35.92	11.91	0.62	38.38	8.89	0.59	0.57	0.96	1.08
Na_2SiO_3	46.21	–	–	–	–	–	50.83	–	–

Table 2. Key physical characteristics of binder components.

Binders	Specific Gravity (gr/cm^3)	Fineness, Blaine (cm^2/gr)	Setting time (min)		Compressive strength (kg/cm^2)		Residue on 45 μm Sieve (%)	Activity Index (%)		Water Insoluble materials (%)
			Initial	Final	7 day	28 day		7 day	28 day	
OPC	3.14	3350	195	270	360	428	–	–	–	–
GGBFS	2.82	4010	–	–	–	–	8.0	88	108	–
Na_2SiO_3	1.20	–	–	–	–	–	–	–	–	0.12

Table 3. Mix design components.

Mix ID	Cement (kg/m^3)	Slag (kg/m^3)	Na_2SiO_3 (kg/m^3)	Fine SSD (kg/m^3)	Coarse SSD (kg/m^3)	W/B	Concrete temperature (°C)
OPCC	450.0	–	–	1001.0	539.0	0.52	23.1
O-AAS	–	405.0	45.0	975.0	525.0	0.52	26.1

for all mixtures. Given the relatively lower water demand of slag compared to Portland cement, the workability of O-AAS differs from that of OPCC under identical water-to-binder (w/b) and binder content. However, since the primary objective of this study was the effect of curing duration on the hardened-state properties, rather than to optimize mixture proportions or assess fresh-state behaviours, the workability of the mixtures was not evaluated. The mix proportions are presented in Table 3.

A laboratory-scale paddle mixer was used to carry out the mixing process. Following the mixing process, the temperature of the freshly prepared concrete was documented, after which the material was poured into casting forms. These forms were then transferred to a moisture-saturated chamber (RH ≥90%) for an initial 24-hour curing phase.

2.2.1. Curing conditions

After the demoulding process, the specimens were then stored according to five distinct curing regimes, which are detailed in Table 4. Cubic, cylindrical, and prismatic specimens were stored in saturated alkaline solution for the periods specified in Table 4 after demolding. Moist curing for standard specimens was performed via immersion in alkaline solutions. Saturated calcium hydroxide solution for OPCC per ASTM C157 [12], and 10% sodium metasilicate solution for O-AAS were selected. This curing protocol for O-AAS was specifically chosen to prevent leaching of critical alkaline activator ions and maintain reaction continuity. Immersion in neutral pH water would establish a concentration gradient, driving outward diffusion of these ions from the concrete matrix

Table 4. Curing conditions of specimens from demoulding until the time of testing.

Code	W360	W0A	W6A	W27A	W55A
Immersed in saturated alkaline solution (days)	Up to 360	0	6	27	55
Unsaturated environment (50 % RH at 23 °C) (days)	0	Up to 360	Up to 360	Up to 360	Up to 360

and depleting internal alkalinity, thereby disrupting the kinetics of slag geopolymerization. Crucially, matching the sodium metasilicate concentration in the curing solution to that within the concrete matrix eliminates this chemical potential gradient, preventing ion migration from the bulk paste. This precise chemical equilibrium sustains the elevated pH and ionic environment required for continuous slag reaction progression throughout the curing period [23].

The unsaturated environmental conditions, consisting of 50 ± 4% relative humidity and 23 ± 2 °C temperature, were set in accordance with the air storage conditions for specimens specified in the ASTM C157 [12].

Due to the impracticality of fully immersing the restrained shrinkage specimens and concrete columns in alkaline solution, an alternative wet-covering method was employed. It should be noted that wet-covering methods are also commonly employed in real-world construction practices for curing concrete structures. The specimens were wrapped with linen cloths thoroughly saturated with either saturated calcium hydroxide solution (for OPCC) or 10% sodium metasilicate solution (for O-AAS), and subsequently sealed with polyethylene sheeting to minimize evaporation. To maintain consistent alkaline conditions,

the cloths were re-wetted with the respective alkaline solutions at least four times per 24-hour period. After the designated curing duration, the wet coverings were removed, and the specimens were exposed to unsaturated environmental conditions (50 ± 4% RH, 23 ± 2 °C) for subsequent drying and monitoring.

2.2.2. Testing procedures

The compressive strength test was carried out in accordance with BS EN 12390-3 [24] on three 100×100 ×100 mm cubic specimens at ages of 7, 28, 56, 90, 180 and 360 days. The test was carried out on specimens stored at five curing conditions as specified in Table 4.

The rapid chloride migration test (RCMT) was carried out in accordance with NT Build 492 [25]. The test was conducted on three disc-shaped specimens, each 50 mm thick and 100 mm in diameter, which were cut from 100 × 200 mm cylindrical specimens. The test was carried out at ages of 28, 56, 90, 180 and 360 days. The test was carried out on specimens stored at 5 curing conditions as specified in Table 4.

For specimens that were in saturated conditions until the test age, according to the standard, a 25 mm disk was first removed from the trowelled surface of the cylinder and set aside. Then, a 50 mm thick disk was prepared from the remaining portion for testing. The disks were saturated and the test was performed according to the standard procedure.

However, for specimens that were in unsaturated conditions before reaching the test age, some changes were made to the cutting method. After the initial curing was completed and the cylindrical specimen was removed from the alkaline solution, a 25 mm thick disc was immediately cut from the trowelled surface of the 100×200 mm cylinder and set aside. The remaining part of the cylinder was kept in the unsaturated environment until the test was performed. At the time of the test, a 50 mm thick disc was cut from the remaining part of the cylinder from the previously cut surface. The prepared discs were then saturated according to the NT Build 492 [25] and subjected to the RCMT test.

According to NT Build 492, a 25-mm surface layer is typically removed to minimize the influence of finishing- or bleeding-induced segregation, thereby ensuring that permeability reflects the internal concrete quality. However, one of the objectives of this study is to assess how an unsaturated environment affects concrete permeability, specifically through surface microcracks induced by drying shrinkage. For specimens exposed in an unsaturated environment, if the surface layer were removed at the standard time (i.e., just before the RCMT test), some of these environmentally induced microcracks might be eliminated. To preserve and evaluate these cracks, the cutting protocol was modified, and the first 25-mm layer was removed immediately after alkaline curing, before exposure to the unsaturated environment. As a result, the newly exposed surface underwent drying shrinkage under unsaturated conditions, allowing shrinkage-induced microcracks to develop — and subsequently influence chloride ingress during the RCMT.

Free shrinkage due to drying was measured according to ASTM C157 [12], using three prismatic specimens (75 × 75 × 285 mm) per mix. To assess the influence of curing duration on free shrinkage development, the standard 28-day saturated moist curing period (per ASTM C157 [12]) was modified. Instead, four distinct curing regimes were applied: W0A, W6A, W27A, and W55A (see Table 4). After the respective moist curing periods, specimens were transferred to an unsaturated environment (50 ± 4% RH, 23 ± 2 °C) at ages of 1, 7, 28, and 56 days. Shrinkage measurements were recorded from the onset of drying exposure, following the guidance in ASTM C596 [26], to enable direct comparison of free shrinkage response under unsaturated conditions.

The confined shrinkage test of concrete was performed according to ASTM C1581 [27] on two circular specimens of each mixture with an outer diameter of 405 mm, an inner diameter of 325 mm, and a thickness of 150 mm. Fig. 1 shows the schematic dimensions of the specimen and the image of the concrete specimen during the confined shrinkage test. This test was performed on specimens stored under two curing conditions, W0A and W6A (Table 4). In this test, the period of exposure of the specimens in unsaturated conditions was limited to a maximum age of 28 days according to the standard. Based on the time of initial crack appearance, the concretes were classified in terms of cracking potential. It should be noted that the storage conditions in W0A were fully in accordance with the requirements of ASTM C1581 [27]; while in W6A, the curing time in a saturated environment was increased compared to the standard. This change was made in order to investigate the effect of increasing the curing time on the crack initiation time and crack width of the concrete.

To evaluate microcracks penetrating the inner concrete layers—and how curing duration affects the durability and strength of the inner concrete—two concrete columns (250 × 250 × 500 mm) were cast per mix and subjected to three curing regimes: W0A, W6A, and W360 (Table 4). It should be noted that the cross-sectional dimensions of these columns largely reflect those found in real structural applications, suggesting that the development and propagation of shrinkage-induced microcracks would closely approximate field conditions. However, since core sampling exclusively evaluated the internal

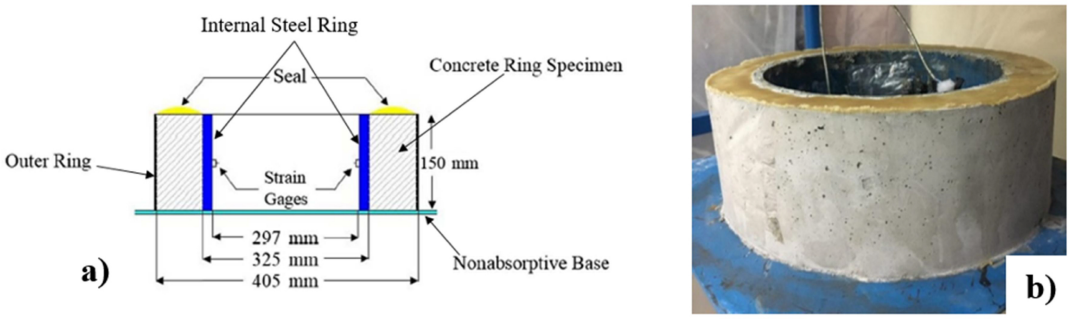

Fig. 1. a) Schematic view of specimen dimensions b) Concrete ring tested under unsaturated conditions in accordance with ASTM C1581 [27].

concrete regions, the surface layer condition remains unassessed, thereby limiting the analysis to the internal concrete performance only. Coring was performed at 360 days. From each column, an initial core of approximately 100 mm in diameter and 80 mm in height was extracted from the trowelled surface and discarded, thereby removing the near-surface zone. Two additional cores (approximately 110 mm and 200 mm in length) were then obtained from deeper regions. Since these inner cores originated well below the surface—i.e., free from finishing- or drying-induced surface effects—the standard 25-mm surface-layer removal prescribed in NT Build 492 [25] was not applied. Instead, 50 mm-thick disc specimens were cut directly from the extracted cores for chloride migration testing. A total of four cores were obtained per mix per curing condition. From these, three cylindrical specimens (for compressive strength, per ASTM C42 [28]) and three disc specimens (for chloride diffusion, per NT Build 492 [25]) were prepared. The coring layout and the moist-curing setup for the columns are illustrated in Fig. 2. An overview of specimen counts, test standards, and method deviations from standard is provided in Table 5.

Microstructural examination was performed qualitatively to illustrate—not quantify— microcracks. A 20 mm-thick disk was cut from 90 mm below the trowelled surface of cylindrical specimens (Ø100 × 200 mm) cured under W27A conditions. An Ogawa Seiki stereo optical microscope at 18× magnification (reflected light) captured representative images. Critically, these images serve solely to provide visual context; no quantitative analysis of crack length, width, or spatial distribution was conducted.

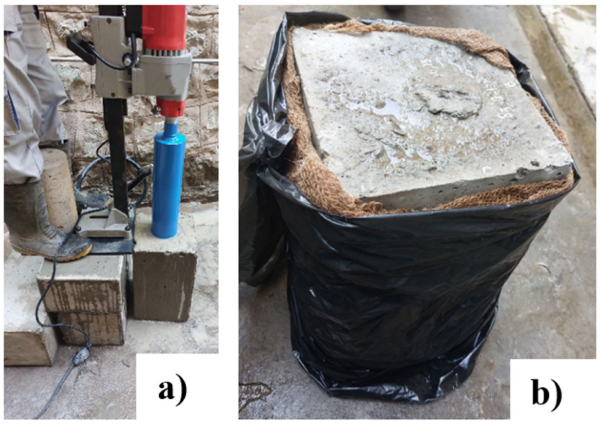

Fig. 2. a) Core sampling operation from a concrete column, b) wet curing of specimens.

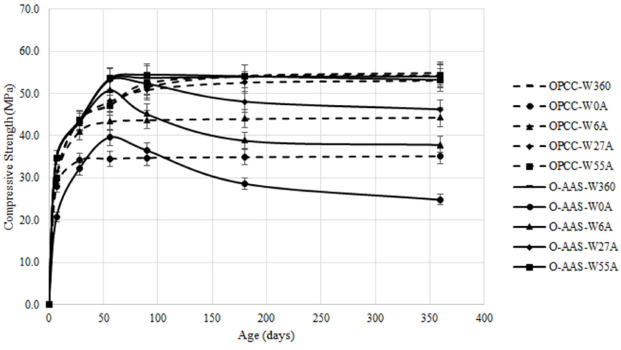

Fig. 3. Compressive strength development of OPCC and O-AAS under five curing regimes (W0A, W6A, W27A, W55A, W360) from 7 to 360 days. Data are means of n = 3 cubic specimens (100 × 100 × 100 mm), tested per BS EN 12390-3 [24].

3. Results and discussions

3.1. Compressive strength

O-AAS formulation targeted 28-day compressive strength values matching those of alkaline-cured OPCC (Fig. 3). This design allows for a direct comparison of their long-term performance under equivalent exposure conditions.

When subjected to W360, the compressive strength of OPCC developed from 30.1 MPa after one week to 54.8 MPa following a full year of curing, with most strength gains occurring within the first 28 days. The increment between 180 and 360 days was less

Table 5. Summary of tests performed.

Test	Number of specimens at each age	Standard Method	Modification to Standard Procedure	Curing Regime
Compressive Strength	3	BS EN 12390-3 [24]	-	W0A-W6A-W27A-W55A-w360
Chloride Ion Diffusion Coefficient	3	NT Build 492 [25]	Early removal of 25 mm surface layer to preserve drying-induced microcracks for realistic chloride ingress assessment under unsaturated conditions.	
Free Shrinkage	3	ASTM C157 [12]	Shorter or extended saturated curing duration from the curing of this standard to assess the effect of curing time on free shrinkage.	W0A-W6A-W27A-W55A
Restrained Shrinkage	2	ASTM C1581 [27]	Prolonged saturated curing duration to assess the influence of curing duration on cracking time and width.	W0A-W6A
Compressive Strength of core specimens	3	ASTM C42 [28]	-	W0A-W6A-w360
Chloride Ion Diffusion Coefficient of specimens	3	NT Build 492 [25]	Core extraction from internal zones to assess microcracking in subsurface layers resulting from variations in curing duration.	

than 2%, indicating stabilization. Similarly, mixtures cured under W27A and W55A showed strength stabilization beyond 180 days, attributed to near complete hydration and reduced reactivity [29]. Conversely, early exposure to unsaturated conditions (W0A and W6A) led to notably lower strength levels and minimal gains after 90 days, likely due to limited internal moisture hindering hydration [15, 29]. Crucially, no long-term strength degradation was observed for OPCC under any curing condition.

In contrast, O-AAS demonstrated a marked sensitivity to curing duration, with strength development diverging significantly from OPCC when moist curing was insufficient.

Under continuous moist curing (W360), O-AAS exhibited compressive strength development analogous to OPCC—increasing from 34.8 MPa at 7 days to 53.5 MPa at 56 days before stabilizing—confirming that saturated conditions enable complete reaction kinetics and long-term structural stability in both systems. Critically, premature drying triggers a distinct degradation mode absent in OPCC: "compressive strength aging," characterized by an irreversible decline in strength after peak. The most severe case (W0A; 0 days initial moist curing) exemplifies this mechanism: strength peaked at 39.6 MPa (56 days) but plummeted by 37.4% (to 24.8 MPa) by 360 days—a deterioration directly attributable to shrinkage-induced microcracking [17–19]. Early-age strength gains initially mask this vulnerability; rapid hydration and geopolymerization temporarily suppresses the propagation of the crack. However, as reaction kinetics decelerate and internal relative humidity drops, capillary tensile stresses exceed the immature binder's tensile strength, propagating microcracks that progressively impair load transfer [7]. Degradation ceases only when hygral equilibrium is reached with the environment. Analyses confirm that the C-A-S-H binder in slag-based systems remains chemically stable during drying [30]. This indicates that the observed strength loss is purely physical—a critical distinction from some alkali-activated systems using other precursors like metakaolin. Importantly, this progressive compressive strength reduction (strength-aging) has been exclusively reported in alkali-activated systems utilizing slag as the precursor material; no comparable loss in strength has been documented to date in systems based on alternative precursors (e.g., natural pozzolans) [8, 30, 31].

The severity of aging is curing-duration-dependent: extending initial moist curing from 0 days (W0A: 37.4% loss) to 6 days (W6A: 25.4% loss) and 27 days (W27A: 13.0% loss) progressively suppresses degradation, while curing for 55 days (W55A) eliminates it. This demonstrates that strength aging is not an intrinsic limitation of O-AAS but a preventable consequence of insufficient early-age moisture retention. Consequently, field implementation requires redefining curing protocols—not material rejection—with a

Table 6. Summary of one-way ANOVA and post hoc (Duncan) results for 360-day compressive strength.

Parameter	OPCC	O-AAS
Levene's test (homogeneity)	$F = 2.202$, $p = 0.117$	$F = 0.849$, $p = 0.525$
ANOVA (between-group effect)	$F(4,10) = 283.4$, $p < 0.001$, $\eta^2 = 0.991$	$F(4,10) = 261.0$, $p < 0.001$, $\eta^2 = 0.991$
Curing regimes significantly < W360	W0A, W6A	W0A, W6A, W27A
Curing regimes not significantly different from W360	W27A, W55A ($p = 0.061$)	W55A ($p = 0.371$)

minimum moist curing threshold to ensure that the matrix requirement strength is achieved before unsaturated environmental exposure.

One-way ANOVA confirmed a highly significant effect of curing duration on 360-day compressive strength for both OPCC ($F(4,10) = 283.4$, p (P-value or Sig.) < 0.001, $\eta^2 = 0.991$) and O-AAS ($F(4,10) = 261.0$, $p < 0.001$, $\eta^2 = 0.991$), with homogeneity of variances verified by Levene's test ($p = 0.117$ for OPCC; $p = 0.525$ for O-AAS, both > 0.05). A summary of the ANOVA outcomes is provided in Table 6, and the full statistical outputs—including Levene's test, ANOVA tables, and Duncan's post hoc groupings—for OPCC and O-AAS are reported in Appendix A (Tables A1 and A2), respectively.

Duncan's post hoc test ($\alpha = 0.05$, $n = 3$) showed that, for both binder systems, W0A and W6A differed significantly from W360 ($p < 0.001$), whereas W27A and W55A did not differ significantly from W360 ($p = 0.061$ for OPCC; $p = 0.371$ for O-AAS). In OPCC, W360 (54.8 MPa), W27A (53.1 MPa), and W55A (54.2 MPa) formed a homogeneous subset (Subset 3). In O-AAS, W360 (54.1 MPa) and W55A (53.1 MPa) were statistically equivalent (Subset 4).

The optimal curing durations for long-term strength retention were determined through statistical comparison to the continuously moist-cured benchmark (W360). For OPCC, the W27A regime preserved mechanical stability, yielding compressive strength statistically equivalent to W360 (53.1 vs. 54.8 MPa, p=0.061). For O-AAS, the W55A regime (55 days) achieved equivalent performance (53.1 vs. 54.1 MPa, p=0.371), eliminating the strength-aging phenomenon.

The ratio of optimal curing durations (O-AAS to OPCC) of approximately 2:1 (55 days vs. 27 days) observed in standardized 100-mm cubic specimens provides a practical scaling factor for field applications. Although specimen geometry may influence absolute curing requirements, decades of structural validation confirm reliable correlation between laboratory specimens and in-situ OPCC performance [29]. Given the concurrent evaluation of both systems under identical conditions, this ratio can serve as an initial guideline for O-AAS by doubling existing OPCC curing durations specified in standards.

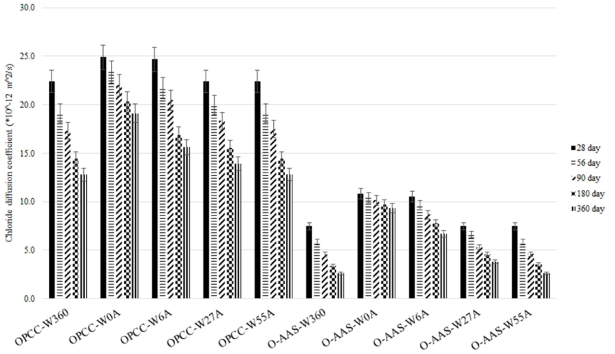

Fig. 4. Non-steady-state chloride diffusion coefficient ($D_{nssm} \times 10^{-12}$ m^2/s) of OPCC and O-AAS under five curing regimes (W0A, W6A, W27A, W55A, W360) at 28–360 days. Data are means of n = 3 disc specimens (Ø100 × 50 mm), tested per NT Build 492 [25].

However, this study does not quantify scale effects for complex structural elements (e.g., beams, slabs) where thermal gradients and restraint conditions differ significantly from cubic specimens. Consequently, site-specific validation through pilot testing on representative elements is essential before full-scale implementation, particularly for critical infrastructure in aggressive environments where premature drying could trigger strength-aging in O-AAS.

For field curing of O-AAS elements, preliminary studies suggest that activator-matched solutions may better preserve interfacial chemistry compared to plain water [23]. However, comprehensive validation under field conditions requires further investigation. Until such data are available, doubling established OPCC curing durations provides a conservative initial approach for non-critical elements.

3.2. Chloride ion diffusion coefficient

Results show a gradual decrease in diffusion coefficients with increasing specimen age, up to 360 days, across all curing regimes (Fig. 4). Exposure to unsaturated environments led to elevated diffusion coefficients for both OPCC and O-AAS mixtures; however, this increase was pronounced in O-AAS. This highlights the greater sensitivity of O-AAS to curing duration concerning its resistance to chloride ingress.

In OPCC specimens cured continuously under saturated alkaline conditions (W360), the chloride migration coefficient reduced from 22.4×10^{-12} m^2/s at 28 days to 12.8×10^{-12} m^2/s at 360 days. A comparable trend was noted for O-AAS, where the coefficient declined from $7.5 \times 10^{-12} \times m^2/s$ at 28 days to 2.6×10^{-12} m^2/s at 360 days. Notably, at both 28 and 360 days, O-AAS exhibited 67% and 80% lower diffusion coefficients, respectively, compared to OPCC, underscoring its superior long-term impermeability under optimal curing. The lower non-steady-state chloride diffusion coefficient (D_{nssm}) of O-AAS compared to OPCC is primarily attributable to its refined and discontinuous capillary pore structure, which impedes chloride ion transport pathways [6, 7]. These findings align with prior research. Bondar et al. [32] found that AAS samples with equivalent 28-day compressive strength to OPCC showed chloride diffusion coefficients reduced by approximately 67%. Similarly, Fan et al. [33] documented a 73% reduction in chloride diffusion for AAS systems compared to OPCC at equivalent water-to-binder ratios.

The non-steady-state chloride diffusion coefficient (D_{nssm}) of O-AAS shows extreme curing sensitivity. With extended moist curing, its performance transforms from inferior to superior compared to OPCC. OPCC showed a steady reduction in permeability from its saturated state (W360) between 28– 360 days: 23.3% (W0A), 36.7% (W6A), 38.0% (W27A), and 42.8% (W55A). O-AAS exhibited a dramatic inversion. Under poor curing (W0A), the reduction reached only 13.9% which is worse than that of OPCC. With adequate curing (W55A), it achieved a 64.7% reduction in D_{nssm}, which is 51% lower than that of OPCC. This nonlinear response is attributed to O-AAS's higher shrinkage [10]. Without sufficient early moisture, this shrinkage generates extensive microcracks [18, 19].

Two mechanisms govern this behaviour. Prolonged moist curing develops matrix tensile strength. This strength resists drying-induced tensile stresses. Aging progressively segments microcrack networks through ongoing geopolymerization. Permeability depends on crack connectivity—not simply on whether cracks are present [7, 16, 19, 34]. Thus, D_{nssm} improves with age even in poorly cured samples. Between 28–360 days, W0A and W6A show 18% and 32% reduction, respectively, despite existing microcracks. Unlike compressive strength—which exhibits precursor-dependent aging behavior (significant degradation only in slag systems), chloride permeability reduction follows similar kinetics across alkali-activated systems with different precursors, as evidenced by comparable trends in slag-based [16] and natural pozzolan-based [31] concretes under identical unsaturated exposure conditions.

Statistical analysis defined the minimum curing threshold; a summary of the results is shown in Table 7, and the full statistical outputs—including Levene's test, ANOVA tables, and Duncan's post hoc groupings—for OPCC and O-AAS are reported in Appendix B (Tables B.1 and B.2), respectively. One-way ANOVA with Duncan's test ($\alpha = 0.05$) confirmed only W55A matched W360 for O-AAS ($p = 0.951$). W0A, W6A, and W27A differed significantly ($p < 0.001$). Their D_{nssm} values were 3.58, 2.55, and 1.46 times W360 (2.61×10^{-12} m^2/s). OPCC followed similar trends: W55A matched W360 ($p = 0.948$), but W0A (+49%), W6A (+22%), and W27A (+9%) were higher.

O-AAS requires 55 days of initial moist curing for optimal durability. This threshold is twice the conventional standard for OPCC. Below this duration, microcrack networks dominate transport properties. They override the intrinsically refined pore structure of slag binder. Field applications must adopt extended curing protocols to unlock O-AAS's permeability advantage.

3.3. Free shrinkage

Across all curing regimes, O-AAS exhibited substantially higher free shrinkage compared to OPCC (Fig. 5). At 360 days, the free shrinkage of O-AAS under the W0A, W6A, W27A, and W55A regimes was approximately 2.56, 2.38, 2.21, and 2.01 times greater, respectively, than that of OPCC. These findings align with previous studies reporting free shrinkage values ranging from 1200 to 1900 $\mu\epsilon$ at 90 days in O-AAS specimens subjected to only one day of curing [35].

The pronounced shrinkage behaviour of O-AAS is primarily attributed to the intrinsic characteristics of its binder system—namely, the viscoelastic nature

Table 7. Summary of one-way ANOVA and post hoc (Duncan) results for 360-day Non-steady-state chloride diffusion coefficient.

Parameter	OPCC	O-AAS
Levene's test (homogeneity)	$F = 0.942$, $p = 0.479$	$F = 2.241$, $p = 0.137$
ANOVA (between-group effect)	$F(4,10) = 115.91$, $p < 0.001$, $\eta^2 = 0.979$	$F(4,10) = 76.14$, $p < 0.001$, $\eta^2 = 0.968$
Curing regimes significantly < W360	W0A, W6A, W27A	W0A, W6A, W27A
Curing regimes not significantly different from W360	W55A ($p = 0.948$)	W55A ($p = 0.951$)

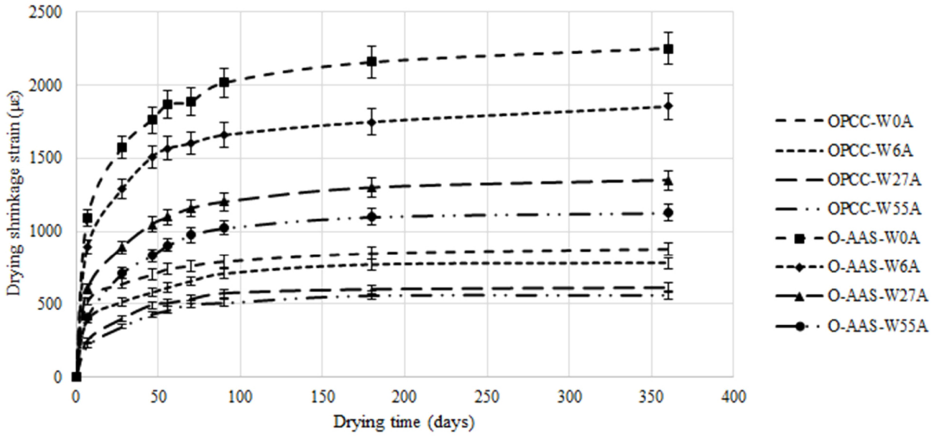

Fig. 5. Free shrinkage strain development ($\mu\epsilon$) of OPCC and O-AAS under four curing regimes (W0A, W6A, W27A, W55A) in unsaturated conditions (50 ± 4% RH, 23 ± 2 °C) over 360 days. Shrinkage was measured from the onset of drying exposure. Data are means of n = 3 prisms (75 × 75 × 285 mm), tested per ASTM C157 [12].

of the C-A-S-H phase, a densely packed pore structure, and heightened capillary pressures resulting from elevated surface tension in the alkaline pore environment. These features are direct outcomes of the accelerated reaction kinetics typical of slag-based materials [36].

Extending the initial curing period prior to exposure to 50% relative humidity significantly reduced drying-induced shrinkage for both concrete types. Specifically, for OPCC, the 360-day free shrinkage under W0A, W6A, and W27A curing regimes increased by approximately 57%, 39%, and 9%, respectively, compared to specimens cured under W55A. These empirical results show good agreement with predictions from the ACI 209 model, which estimates increases of 60%, 33%, and 15% under analogous curing durations [37].

However, findings from other studies differ. For instance, Bagheri et al. [38] observed only an 11% increase in free shrinkage of OPCC when curing duration was extended from one to seven days. This discrepancy may be attributed to variations in the water-to-cement ratio or binder composition.

For O-AAS, the 360-day free shrinkage under W0A, W6A, and W27A exceeded that of W55A by 72%, 58%, and 17%, respectively. Across all curing regimes, O-AAS exhibited 2.0 to 2.6 times higher free shrinkage than OPCC at 360 days (Fig. 5). Specifically, the ratio was 2.56, 2.38, 2.21, and 2.01 for W0A, W6A, W27A, and W55A, respectively. The present findings highlight the importance of early-age curing in mitigating shrinkage in O-AAS. This aligns with the work of Aiken et al. [39], who observed a 48% decrease in free shrinkage for fly ash-based alkali-activated concrete when curing duration was extended from one to twenty-one days.

3.4. Restrained shrinkage

Only the W0A and W6A curing conditions were assessed for both OPCC and O-AAS (Table 8). All mixtures exhibited a pronounced tendency toward early-age cracking, with O-AAS demonstrating considerably greater susceptibility compared to OPCC. Crack initiation was observed at notably earlier stages in O-AAS, with visible cracks forming in the W0A specimen within merely 20 minutes of exposure to a 50% relative humidity environment. This accelerated crack development is primarily due to the synergistic effects of autogenous shrinkage and drying-induced tensile stresses.

Unlike OPCC, O-AAS experiences considerably higher autogenous shrinkage. Li et al. [40] reported visible cracking in alkali-activated slag paste as early as 12.3 hours after casting under ring test conditions, even in the absence of drying. These findings illustrate the rapid build-up of internal tensile stresses in alkali-activated slag systems due to intense self-desiccation. When drying stresses are superimposed on autogenous shrinkage, crack initiation accelerates further.

Average crack width was calculated by measuring ten equally spaced points along each visible crack at 28 days. The divergent response of crack width to curing duration in OPCC versus O-AAS stems from fundamental differences in their time-dependent mechanical properties. While O-AAS exhibits wider cracks than OPCC (7.86 mm vs. 1.23 mm under W0A) due to its higher free shrinkage (Section 3.3), the two systems respond oppositely to extended curing—a phenomenon governed by their elastic and viscoelastic characteristics at the cracking age.

Table 8. Results of the restrained shrinkage test for OPCC and O-AAS under two curing regimes (W0A, W6A).

Mix ID	Cracking Age (*days*)	Net Cracking Age (*days*)	Cracking Potential	Average Crack Width at 28 Days (*mm*)
OPCC-W0A	7.48	6.48	H	1.23
OPCC-W6A	12.26	5.26	H	2.15
O-AAS-W0A	1.01	0.01	H	7.86
O-AAS-W6A	7.06	0.06	H	3.46

Data reported mean values of n = 2 ring-shaped specimens (outer Ø405 mm, inner Ø325 mm, thickness 150 mm) per mixture and regime, tested in accordance with ASTM C1581 [27].

In OPCC, prolonged curing (W6A) increases the crack width by 74.8% (from 1.23 mm to 2.15 mm), despite delaying the onset of cracking (from 7.48 to 12.26 days). This behavior arises from two synergistic mechanisms: (i) elastic modulus development between 7–12 days, which amplifies tensile stresses at the steel ring interface; and (ii) pore structure refinement that intensifies capillary tension during drying. Although extended curing enhances tensile strength, the concurrent rise in stiffness and capillary stresses dominates fracture behavior—concentrating energy release into fewer, wider cracks upon failure [38].

Conversely, O-AAS exhibited a 56.0% reduction in crack width with extended curing (from 7.86 to 3.46 mm), attributable to its superior stress-relief capacity. Three factors govern this response: (i) limited elastic modulus evolution between 1–7 days, reducing stress amplification at the steel ring interface; (ii) higher creep compliance, which enables continuous stress relaxation during drying; and (iii) the reduced free shrinkage magnitude of O-AAS under W6A compared to W0A, which decreases the driving force for wider crack propagation [39].

Despite benefits from extended curing, O-AAS remains highly vulnerable to early-age cracking. Both W0A and W6A curing regimes proved insufficient to suppress microcracking effectively.

3.5. Core test results

To investigate the effect of curing duration on compressive strength and chloride resistance, core samples were extracted from the inner concrete layers. This was done to evaluate the potential susceptibility of the internal structural concrete (Table 9).

A comparative evaluation of the chloride diffusion coefficients obtained from W360 cores and standard cylindrical specimens (see Section 3.2) reveals a high level of agreement, which suggests that the core extraction procedure does not materially impact the ion transport characteristics. Similarly, after adjusting for specimen geometry, the compressive strength values of W360 cores closely matched those of corresponding standard specimens reported in Section 3.1. These results validate core-based testing as a reliable and practical method for assessing the in-situ mechanical and durability performance within the internal regions of real-scale structural elements.

Table 9. Core test results at 360 days for OPCC and O-AAS under three curing regimes (W0A, W6A, W360).

Mix ID	Compressive strength (*MPa*)	Chloride ion diffusion coefficient ($\times 10^{-12} m^2/s$)
OPCC-W360	44.7	13.05
OPCC-W0A	44.2	13.47
OPCC-W6A	44.5	13.24
O-AAS-W360	44.1	2.66
O-AAS-W0A	41.0	3.41
O-AAS-W6A	43.9	2.67

Compressive strength: Data reported mean values of n = 3 cylindrical cores tested per ASTM C42 [28]; and Chloride diffusion coefficient (Dnssm $\times 10^{-12}$ m^2/s): Data reported mean values of n = 3 disk specimens tested per NT Build 492 [25].

The consistency between laboratory specimen behavior and core test results from structural columns (250×250×500 mm) confirms that the fundamental degradation mechanisms in O-AAS are scale-independent phenomena. While absolute crack widths and permeability values will vary with structural geometry and restraint conditions in field applications, the relative vulnerability of O-AAS compared to OPCC — and the proportionally longer curing required to mitigate this vulnerability — represents an intrinsic material characteristic that transcends specimen size. This comparative approach provides a reliable framework for engineers to anticipate O-AAS performance in real structures, while acknowledging that quantitative predictions require project-specific validation.

A one-way ANOVA, with post hoc comparisons performed using Duncan's test at a 95% confidence level, was conducted to evaluate the effect of early-age curing (W0A, W6A, W360) on the core properties of OPCC and O-AAS at 360 days. Summary statistics of the ANOVA for compressive strength and chloride diffusion coefficient are presented in

Table 10. Summary of one-way ANOVA and Duncan post hoc results for the 360-day compressive strength in concrete cores.

Parameter	OPCC	O-AAS
Levene's test (homogeneity)	$F = 1.083$, $p = 0.397$	$F = 1.164$, $p = 0.374$
ANOVA (between-group effect)	$F(2,6) = 0.239$, $p = 0.794$, $\eta^2 = 0.074$	$F(2,6) = 7.551.0$, $p = 0.023$, $\eta^2 = 0.716$
Curing regimes significantly < W360	–	W0A
Curing regimes not significantly different from W360	W0A, W6A ($p = 0.061$)	W6A ($p = 0.371$)

Table 11. Summary of one-way ANOVA and Duncan post hoc results for the 360-day Non-steady-state chloride diffusion coefficient in concrete cores.

Parameter	OPCC	O-AAS
Levene's test (homogeneity)	$F = 0.\ 0.223$, $p = 0.806$	$F = 0.256$, $p = 0.782$
ANOVA (between-group effect)	$F(2,6) = 0.341$, $p = 0.724$, $\eta^2 = 0.102$	$F(2,6) = 8.366$, $p = 0.018$, $\eta^2 = 0.722$
Curing regimes significantly < W360	–	W0A
Curing regimes not significantly different from W360	W0A, W6A ($p = 0.061$)	W6A ($p = 0.964$)

Tables 10 and 11, respectively, while the full statistical outputs for OPCC and O-AAS are detailed in Tables C.1 and C.3 and Tables C.2 and C.4 (Appendix C).

For OPCC, no significant differences were observed in either 360-day core compressive strength ($F(2,6) = 0.239$, $p = 0.794$) or chloride diffusion coefficient ($F(2,6) = 0.341$, $p = 0.724$) across W0A, W6A, and W360 curing regimes (Duncan's $p = 0.061$ in both cases). Mean compressive strengths ranged narrowly from 44.2 to 44.7 MPa, while diffusion coefficients varied only from 13.05×10^{-12} m^2/s to 13.47×10^{-12} m^2/s—all within a single homogeneous subset. This indicates that microcracks induced by early unsaturated exposure in OPCC remain predominantly superficial and do not significantly penetrate or degrade the internal matrix. Nevertheless, overlooking such surface-level deterioration in durability assessment may lead to overestimated service-life predictions, as surface-connected cracks—though not reflected in core tests—can accelerate the ingress of aggressive species and reduce the effective cover depth in real structural elements.

In contrast, for O-AAS, curing duration significantly influenced core performance. Although W6A and W360 showed no significant differences in compressive strength ($p = 0.371$) or chloride diffusion ($p = 0.964$), the W0A regime induced statistically significant degradation: compressive strength was 7.1% lower (41.0 MPa vs. 44.1 MPa, $p = 0.023$), and the chloride diffusion coefficient was 28.2% higher (3.41 vs. 2.66×10^{-12} m^2/s, $p = 0.018$) compared to W360. These results confirm that insufficient initial moist curing in O-AAS promotes through-section microcracking via early-age autogenous and drying shrinkage, compromising both mechanical integrity and transport properties. Moreover, extending the initial water curing to 6 days (W6A) was sufficient to achieve performance statistically indistinguishable from continuous 360-day curing, indicating that a one-week initial moist curing period is adequate to ensure stable microstructural development and mitigate crack propagation.

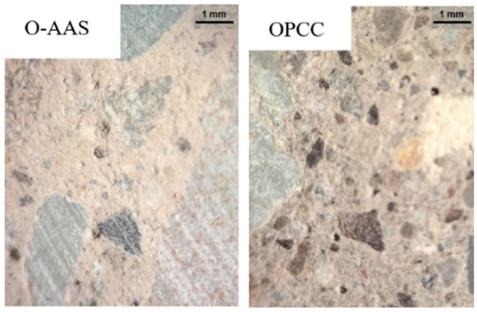

Fig. 6. Optical microscopy images (18×, reflected light) of polished sections cut 90 mm below the trowelled surface of OPCC and O-AAS (W27A regime). Representative images only; no quantitative crack analysis performed.

Overall, these findings underscore that, unlike OPCC, O-AAS is highly sensitive to curing duration; early microcracks penetrate deeper, reducing internal strength and durability. The superior performance of O-AAS under W360 curing arises from its dense microstructure, which effectively limits chloride ingress — achievable only with sufficient curing. Otherwise, insufficient curing results in internal cracking and unreacted phases, significantly compromising durability.

3.6. Visual condition of concrete sections

Optical microscopy provided only qualitative and illustrative evidence of microcracking, without offering quantitative crack metrics. Representative micrographs (Fig. 6) reveal a stark contrast: the OPCC section showed no observable microcracks throughout

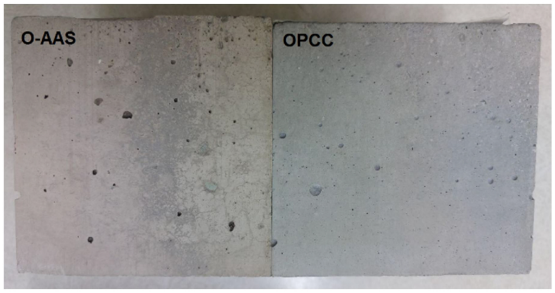

Fig. 7. Visual surface condition of OPCC and O-AAS specimens (W27A, at 360 days). Images illustrate qualitative microcrack patterns; crack dimensions not measured.

the bulk matrix, whereas the O-AAS section exhibited multiple microcracks, especially near the surface. These images serve solely to corroborate the degradation mechanisms discussed in Sections 3.1, 3.2 and 3.5. No measurements of crack length or depth were performed.

Surface examinations of cubic specimens revealed numerous microcracks in W27A-cured O-AAS specimens. This visible damage pattern aligns with the reported strength loss and higher chloride diffusion coefficient, as discussed in Sections 3.1, 3.2 and 3.5. In contrast, OPCC specimens under identical curing conditions showed only limited surface microcracks, as documented in Fig. 7. Rigorous quantification of microcrack characteristics—particularly width, spatial distribution, and connectivity—requires advanced techniques such as scanning electron microscopy (SEM) or crack-depth measurements, as conventional optical microscopy lacks the resolution and depth-sectioning capability for such analyses.

4. Conclusion

This study demonstrates that O-AAS requires significantly longer initial moist curing compared to OPCC to achieve long-term stability under unsaturated conditions. While OPCC maintained stable compressive strength across all curing regimes, O-AAS under insufficient curing conditions (W0A) experienced a phenomenon termed "strength aging"; specifically, under these conditions, the compressive strength decreased by 37% from its maximum value at 56 days (39.6 MPa) to 360 days (24.8 MPa). This phenomenon was directly attributed to microcracking induced by early-age shrinkage.

Insufficient curing (W0A relative to W360) at 360 days resulted in a 3.6-fold increase in chloride diffusion coefficient for O-AAS and a 1.5-fold increase for OPCC; the ratio of these increases indicates that O-AAS is 2.4 times more sensitive to inadequate curing than OPCC in terms of chloride ingress susceptibility. Whereas under optimal curing conditions (W360), the diffusion coefficient of O-AAS at 360 days was 80% lower than that of ordinary Portland cement concrete. Under 360 days of drying conditions, the ratio of free shrinkage in O-AAS under insufficient curing (W0A) to optimal curing (W360) was 2.0, while this ratio for OPCC was 1.5; additionally, the ratio of free shrinkage of O-AAS to OPCC under optimal curing (W360) was calculated as 2.0. In the restrained shrinkage test, extending initial moist curing from W0A to W7A conditions reduced crack width significantly by 56% (from 7.86 mm to 3.46 mm).

Laboratory testing revealed that O-AAS requires 56 days of initial moist curing to completely eliminate strength aging and achieve optimal durability—approximately twice the duration required for OPCC (28 days). This 2:1 curing duration ratio provides a scientific foundation for adapting existing OPCC curing standards to O-AAS. However, field validation under actual service conditions remains essential prior to widespread implementation, particularly for critical infrastructure. Future research should investigate the influence of mixture variables (such as different W/B ratios, varying activator types and varying activator ratios) and environmental factors (such as curing temperatures) on optimal curing protocols for diverse alkali-activated systems.

Acknowledgements

The authors would like to express their sincere gratitude to the staff and personnel of the Concrete Laboratory at Khajeh Nasir Toosi University of Technology for their valuable cooperation and support throughout this research.

Conflict of interest

The authors declared no potential conflicts of interest with respect to the research, authorship, and/or publication of this article.

Data availability statement

All graphs and data obtained or generated during the investigation appear in the published article.

Funding

There was no funding source for this research.

Author's contributions

Ali Sadrmomtazi: Conceptualization, Supervision, Project Administration, Writing – Review & Editing.

Hamed Zanganeh: Investigation, Data Curation, Formal Analysis, Writing – Original Draft, Visualization.

All authors have read and approved the final manuscript.

Ethics

There are no ethical issues with the publication of this manuscript.

References

1. Duzy P, Choinska M, Hager I, Amiri O, Claverie J. Mechanical Strength and Chloride Ions' Penetration of Alkali-Activated Concretes (AAC) with Blended Precursor. *Materials*. 2022;15(13):4475. doi:10.3390/ma15134475
2. Jiang L, Niu Y, Jin W, Gao H, Chen L. Influence of chloride salt type on chloride ion diffusion performance of alkali-activated slag mortar. *Constr Build Mater*. 2022;351:128930. doi:10.1016/j.conbuildmat.2022.128930
3. Nasir M, Mahmood AH, Ashraf A, Bahraq AA. History, recent progress, and future challenges of alkali-activated binders - An overview. *Constr Build Mater*. 2024;426:136141. doi:10.1016/j.conbuildmat.2024.136141
4. Elzeadani M, Bompa DV, Elghazouli AY. One part alkali activated materials: A state-of-the-art review. *J Build Eng*. 2022;57:104871. doi:10.1016/j.jobe.2022.104871
5. Fu Q, Bu M, Zhang Z, Xu W, Yuan Q, Niu D. Hydration Characteristics and Microstructure of Alkali-Activated Slag Concrete: A Review. *Eng*. 2023;20:162-79. doi:10.1016/j.eng.2021.07.026
6. Luukkonen T. Alkali-Activated Materials in Environmental Technology Applications. In: Pacheco-Torgal F, Chindaprasirt P, Ozbakkaloglu T, editors. Handbook of Advances in Alkali-Activated Concrete. Cambridge: Woodhead Publishing; 2022. p. 317-44.
7. Pacheco-Torgal F, Chindaprasirt P, Ozbakkaloglu T, editors. Handbook of advances in Alkali-activated Concrete. Cambridge: Woodhead Publishing; 2021.
8. Barış KE. One-part alkali-activated mortars based on clay brick waste, natural pozzolan waste, and marble powder waste. *Journal of Sustainable Construction Materials and Technologies*. 2024;9(4):Article 7. doi:10.47481/jscmt.1607828
9. Runci A, Serdar M. Effect of curing time on the chloride diffusion of alkali-activated slag. *Case Studies in Construction Materials*. 2022;16:e00927. doi:10.1016/j.cscm.2022.e00927.
10. Amran M, Onaizi AM, Makul N, Abdelgader HS, Tang WC, Alsulami BT, *et al.* Shrinkage mitigation in alkali-activated composites: A comprehensive insight into the potential applications for sustainable construction. *Results Eng*. 2023;20:101452. doi:10.1016/j.rineng.2023.101452
11. Bezemer HJ, Luković M. Early-age and long-term deformations in reinforced slag-based alkali activated concrete. *Construction and Building Materials*. 2025;476:141317. doi:10.1016/j.conbuildmat.2025.141317.
12. ASTM International. Standard test method for length change of hardened cement mortar and concrete. ASTM C157. West Conshohocken, PA: ASTM International; 2023.
13. Sanjuán MA, Muñoz-Martialay R. Influence of the age on air permeability of concrete. *J Mater Sci*. 1995;30(22):5657-62. doi:10.1007/BF00356701
14. Bažant ZP, Raftshol WJ. Effect of cracking in drying and shrinkage specimens. *Cem Concr Res*. 1982;12(2):209-26. doi:10.1016/0008-8846(82)90031-5
15. Arayeshgar M, Madandoust R, Ranjbar MM. A comparative study on superabsorbent polymer (SAP) and recycled lightweight aggregate (LWA) as internal curing agents for high-strength concrete (HSC). *Int J Eng Trans B Appl*. 2025;38(2):452-61. doi:10.5829/IJE.2025.38.02B.18
16. Wardhono A, Gunasekara C, Law DW, Setunge S. Comparison of long term performance between alkali activated slag and fly ash geopolymer concretes. *Constr Build Mater*. 2017;143:272-79. doi:10.1016/j.conbuildmat.2017.03.153
17. Alhamoud A, Riahi HT, Ataei A. Mechanical properties and stress-strain relationship of slag-based one-part geopolymer concrete: A comparative study. *Results Eng*. 2024;24:102952. doi:10.1016/j.rineng.2024.102952
18. Collins FG, Sanjayan JG. Microcracking and strength development of alkali activated slag concrete. *Cem Concr Compos*. 2000;23(4-5):345-52. doi:10.1016/S0958-9465(01)00003-8
19. Prinsse S, Hordijk DA, Ye G, Lagendijk P, Luković M. Time-dependent material properties and reinforced beams behavior of two alkali-activated types of concrete. *Struct Concr*. 2020;21(2):642-58. doi:10.1002/suco.201900235
20. ASTM International. Standard specification for Portland cement. ASTM C150. West Conshohocken, PA: ASTM International; 2023.
21. ASTM International. Standard specification for slag cement for use in concrete and mortars. ASTM C989. West Conshohocken, PA: ASTM International; 2023.
22. ASTM International. Standard specification for concrete aggregates. ASTM C33. West Conshohocken, PA: ASTM International; 2023.
23. Marvila MT, Garcez de Azevedo AR, Linhares Junior JAT, Vieira CMF. Activated alkali cement based on blast furnace slag: effect of curing type and concentration of Na_2O. *J. Mater. Res. Technol.*, 2023;23:4551–4565. https://doi.org/10.1016/j.jmrt.2023.02.088
24. British Standards Institution. Testing hardened concrete - Part 3: Compressive strength of test specimens. BS EN 12390-3. London: British Standards Institution; 2009.
25. Nordic Innovation Centre. Chloride migration coefficient from non-steady state migration experiments. NT Build 492. Espoo: Nordic Innovation Centre; 1999.
26. ASTM International. Standard test method for drying shrinkage of mortar containing hydraulic cement. ASTM C596. West Conshohocken, PA: ASTM International; 2023.
27. ASTM International. Standard test method for determining age at cracking and induced tensile stress characteristics of mortar and concrete under restrained shrinkage. ASTM C1581. West Conshohocken, PA: ASTM International; 2024.
28. ASTM International. Standard test method for obtaining and testing drilled cores and sawed beams of concrete. ASTM C42. West Conshohocken, PA: ASTM International; 2023.
29. Neville AM. Concrete Technology. 2nd ed. New Delhi: Pearson Education India; 2008.
30. Lloyd RR. Accelerated ageing of geopolymers. In: Pacheco-Torgal F, Labrincha JA, Leonelli C, Palomo A, Chindaprasirt P, editors. Geopolymers: Structures, Processing, Properties

and Industrial Applications. Cambridge: Woodhead Publishing; 2009. p. 139-60. doi:10.1533/9781845696382.2.139
31. Barış KE. Development of a self-cured alkali-activated mortar. *Journal of Sustainable Construction Materials and Technologies*. 2025;10(2):Article 9. doi:10.29187/2458-973X.1185
32. Bondar D, Ma Q, Soutsos M, Basheer M, Provis JL, Nanukuttan S. Alkali activated slag concretes designed for a desired slump, strength and chloride diffusivity. *Constr Build Mater*. 2018;190:191-99. doi:10.1016/j.conbuildmat.2018.09.124
33. Fan J, Zhu H, Shi J, Li Z, Yang S. Influence of slag content on the bond strength, chloride penetration resistance, and interface phase evolution of concrete repaired with alkali activated slag/fly ash. *Constr Build Mater*. 2020;263:120639. doi:10.1016/j.conbuildmat.2020.120639
34. Hajibabaee A, Moradllo MK, Behravan A, Ley MT. Quantitative measurements of curing methods for concrete bridge decks. *Constr Build Mater*. 2018;162:306-13. doi:10.1016/j.conbuildmat.2017.12.023
35. Zhou S, Ma C, Long G, Xie Y. A novel non-Portland cementitious material: Mechanical properties, durability and characterization. *Constr Build Mater*. 2020;238:117671. doi:10.1016/j.conbuildmat.2019.117671
36. Coppola L, Coffetti D, Crotti E, Candamano S, Crea F, Gazzaniga G, *et al.* The combined use of admixtures for shrinkage reduction in one-part alkali activated slag-based mortars and pastes. *Constr Build Mater*. 2021;248:118682. doi:10.1016/j.conbuildmat.2020.118682
37. ACI Committee 209. Guide for Modeling and Calculating Shrinkage and Creep in Hardened Concrete. ACI 209.2R-08 (Reapproved 2008). Farmington Hills, MI: American Concrete Institute; 2008.
38. Bagheri AR, Jamali A, Pourmir M, Zanganeh H. The influence of curing time on restrained shrinkage cracking of concrete with shrinkage reducing admixture. *Adv Civ Eng Mater*. 2019;8(1):596-610. doi:10.1520/ACEM20190100
39. Aiken TA, Kwasny J, Zhou Z, McPolin D, Sha W. Factors affecting the drying shrinkage of alkali-activated slag/fly ash mortars. *MRS Adv*. 2023;8(21-22):1266-72. doi:10.1557/s43580-023-00647-6
40. Li Z, Wyrzykowski M, Dong H, Granja J, Azenha M, Lura P, *et al.* Internal curing by superabsorbent polymers in alkali-activated slag. *Cem Concr Res*. 2020;135:106123. doi:10.1016/j.cemconres.2020.106123

Appendix

A. Summary of statistical analysis results: A one-way ANOVA was conducted, and means were compared using Duncan's test to evaluate the effect of curing type on 360-day compressive strength.

Table A1. Comparison of 360-day compressive strength of OPCC under different curing durations.

Statistical Assessment of Variance Homogeneity				
Test	Statistic	df1	df2	Sig.
Levene	2.202	4	10	0.117

Duncan				
		Subset for alpha = 0.05		
Curing	N	1	2	3
W0A	3	35.1		
W6A	3		44.4	
W27A	3			53.1
W55A	3			54.2
W360	3			54.8
Sig.		1.000	1.000	0.061

One-way ANOVA- Compressive					
	Sum of Squares	df	Mean Square	F	Sig.
Between Groups	867.630	4	216.909	283.4	0.000
Within Groups	7.653	10	0.765		
Total	875.289	14			

Table A2. Comparison of 360-day compressive strength of O-AAS under different curing durations.

Statistical Assessment of Variance Homogeneity				
Test	Statistic	df1	df2	Sig.
Levene	0.849	4	10	0.525

Duncan					
		Subset for alpha = 0.05			
Curing	N	1	2	3	4
W0A	3	24.8			
W6A	3		37.9		
W27A	3			46.2	
W55A	3				53.1
W360	3				54.1
Sig.		1.000	1.000	1.000	0.371

One-way ANOVA- Compressive					
	Sum of Squares	df	Mean Square	F	Sig.
Between Groups	1780.969	4	445.243	261.0	0.000
Within Groups	17.060	10	1.706		
Total	1798.029	14			

B. Summary of statistical analysis results: A one-way ANOVA was conducted, and means were compared using Duncan's test to evaluate the Effect of Curing Type on 360-Day Chloride Diffusion Coefficient

Table B.1. Effect of curing type on 360-day chloride diffusion coefficient of OPCC.

Statistical Assessment of Variance Homogeneity					
Test	Statistic	df1	df2	Sig.	
Levene	0.942	4	10	0.479	
Duncan					
		Subset for alpha = 0.05			
Age	N	1	2	3	4
W360	3	12.79			
W55A	3	12.82			
W27A	3		13.91		
W6A	3			15.61	
W0A	3				19.11
Sig.		0.948	1.000	1.000	1.000
One-way ANOVA -Diffusion					
	Sum of Squares	df	Mean Square	F	Sig.
Between Groups	83.885	4	20.971	115.9	0.000
Within Groups	1.809	10	0.181		
Total	85.695	14			

Table B.2. Effect of curing type on 360-day chloride diffusion coefficient of O-AAS.

Statistical Assessment of Variance Homogeneity					
Test	Statistic	df1	df2	Sig.	
Levene	2.241	4	10	0.137	
Duncan					
		Subset for alpha = 0.05			
Age	N	1	2	3	4
W360	3	2.61			
W55A	3	2.64			
W27A	3		3.80		
W6A	3			6.66	
W0A	3				9.34
Sig.		0.951	1.000	1.000	1.000
One-way ANOVA - Diffusion					
	Sum of Squares	df	Mean Square	F	Sig.
Between Groups	102.922	4	25.730	76.1	0.000
Within Groups	3.379	10	0.338		
Total	106.301	14			

C. Summary of statistical analysis results: A one-way ANOVA was conducted, and means were compared using Duncan's test for Comparing the 360-Day Compressive Strength and Chloride Ion Diffusion Coefficient of Cores Under Different Curing Conditions

Table C.1. Comparison of 360-day compressive strength of OPCC cores.

Statistical Assessment of Variance Homogeneity				
Test	Statistic	df1	df2	Sig.
Levene	1.083	2	6	0.397
Duncan				
		Subset for alpha = 0.05		
Curing	N	1		
W0A	3	44.2		
W6A	3	44.5		
W360	3	44.7		
Sig.		0.061		
One-way ANOVA -Compressive				
	Sum of Squares	df	Mean Square	F	Sig.
Between Groups	0.287	2	0.143	0.239	0.794
Within Groups	3.593	6	0.599		
Total	3.880	8			

Table C.2. Comparison of 360-day compressive strength of O-AAS cores.

Statistical Assessment of Variance Homogeneity				
Test	Statistic	df1	df2	Sig.
Levene	1.164	2	6	0.374
Duncan				
		Subset for alpha = 0.05		
Curing	N	1		
W0A	3	41.0		
W6A	3			43.9
W360	3			44.1
Sig.		1.000		0.371
One-way ANOVA -Compressive				
	Sum of Squares	df	Mean Square	F	Sig.
Between Groups	18.107	2	9.053	7.551	0.023
Within Groups	7.193	6	1.199		
Total	25.300	8			

Table C.3. Comparison of 360-day chloride ion diffusion coefficient of OPCC cores.

Statistical Assessment of Variance Homogeneity					
Test	Statistic	df1	df2	Sig.	
Levene	0.223	2	6	0.806	
Duncan					
		Subset for alpha = 0.05			
Curing	N	1			
W360	3	13.05			
W6A	3	13.24			
W0A	3	13.47			
Sig.		0.061			
One-way ANOVA -Diffusion					
	Sum of Squares	df	Mean Square	F	Sig.
Between Groups	0.269	2	0.135	0.341	0.724
Within Groups	2.368	6	0.395		
Total	2.637	8			

Table C.4. Comparison of 360-day chloride ion diffusion coefficient of O-AAS cores.

Statistical Assessment of Variance Homogeneity					
Test	Statistic	df1	df2	Sig.	
Levene	0.256	2	6	0.782	
Duncan					
		Subset for alpha = 0.05			
Curing	N	1			
W360	3	2.66			
W6A	3	2.67			
W0A	3		3.41		
Sig.		0.964	1.000		
One-way ANOVA -Diffusion					
	Sum of Squares	df	Mean Square	F	Sig.
Between Groups	1.120	2	0.560	8.366	0.018
Within Groups	0.402	6	0.067		
Total	1.552	8			